CRREL
REPORT 82-9

US Army Corps of Engineers
Cold Regions Research & Engineering Laboratory

Model study of Port Huron ice control structure

Wind stress simulation

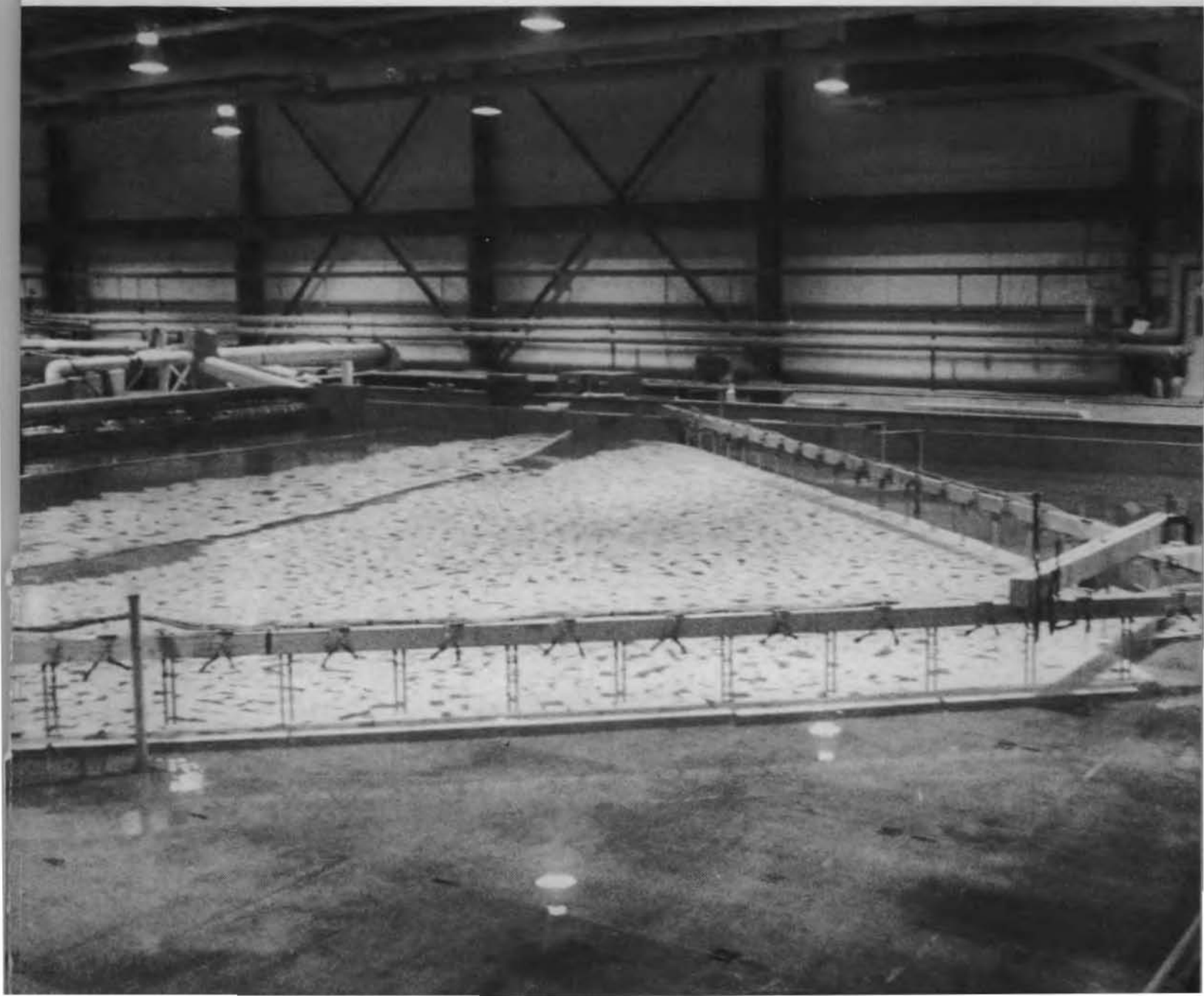

CRREL Report 82-9

April 1982

Model study of Port Huron ice control structure

Wind stress simulation

D.S. Sodhi, D.J. Calkins and D.S. Deck

Prepared for
U.S. ARMY ENGINEER DISTRICT, DETROIT

Unclassified

SECURITY CLASSIFICATION OF THIS PAGE *(When Data Entered)*

REPORT DOCUMENTATION PAGE		READ INSTRUCTIONS BEFORE COMPLETING FORM
1. REPORT NUMBER CRREL Report 82-9	2. GOVT ACCESSION NO.	3. RECIPIENT'S CATALOG NUMBER
4. TITLE *(and Subtitle)* MODEL STUDY OF PORT HURON ICE CONTROL STRUCTURE: WIND STRESS SIMULATION		5. TYPE OF REPORT & PERIOD COVERED 6. PERFORMING ORG. REPORT NUMBER
7. AUTHOR*(s)* D.S. Sodhi, D.J. Calkins and D.S. Deck		8. CONTRACT OR GRANT NUMBER*(s)* NCE-IA-79-081-EK
9. PERFORMING ORGANIZATION NAME AND ADDRESS U.S. Army Cold Regions Research and Engineering Laboratory Hanover, New Hampshire 03755		10. PROGRAM ELEMENT, PROJECT, TASK AREA & WORK UNIT NUMBERS
11. CONTROLLING OFFICE NAME AND ADDRESS U.S. Army Engineer District, Detroit Detroit, Michigan		12. REPORT DATE April 1982 13. NUMBER OF PAGES 36
14. MONITORING AGENCY NAME & ADDRESS*(if different from Controlling Office)*		15. SECURITY CLASS. *(of this report)* Unclassified 15a. DECLASSIFICATION/DOWNGRADING SCHEDULE

16. DISTRIBUTION STATEMENT *(of this Report)*

Approved for public release; distribution unlimited

17. DISTRIBUTION STATEMENT *(of the abstract entered in Block 20, if different from Report)*

18. SUPPLEMENTARY NOTES

19. KEY WORDS *(Continue on reverse side if necessary and identify by block number)*

Great Lakes
Hydraulic models
Ice control
Water flow
Wind shear

20. ABSTRACT *(Continue on reverse side if necessary and identify by block number)*

This study deals with the distribution of forces along the converging boundaries of the Port Huron, Michigan, region where unconsolidated ice in Lake Huron is held against wind and water stresses. An experimental basin was built to induce uniform shear stress on the model ice cover by flowing water beneath the ice. The boundary segments, which held the ice cover in the region, were instrumented to measure force in the normal and tangential directions. The distribution of normal forces along the boundary was compared with a distribution derived by using a theoretical model. An ice control structure (ICS) was installed in the basin and experiments were conducted to measure the forces on the ICS and the ice release through the opening in the ICS during simulated ship passages. The experimental results are presented in a nondimensional form. In addition, the force per unit length on the ICS and the area of ice released through its opening were estimated for the expected wind conditions at the Port Huron site.

DD FORM 1 JAN 73 1473 EDITION OF 1 NOV 65 IS OBSOLETE

Unclassified

SECURITY CLASSIFICATION OF THIS PAGE *(When Data Entered)*

PREFACE

This report was prepared by Dr. D.S. Sodhi, D.J. Calkins, and D.S. Deck, Research Hydraulic Engineers, of the Ice Engineering Research Branch, Experimental Engineering Division, U.S. Army Cold Regions Research and Engineering Laboratory. Funding for this research was provided by U.S. Army Engineer District, Detroit, under Interagency Order NCE-IA-79-081-EK.

Dr. Malcolm Mellor and Steven Daly of CRREL technically reviewed the manuscript of this report.

CONTENTS

ILLUSTRATIONS

TABLES

LIST OF SYMBOLS

a	average floe size
b	size of opening in the ICS
c	cohesive strength of an ice cover (N/m)
d	length of ice cover as defined in Fig. 5
e, ℓ	position of and length of an ICS as defined in Fig. 10
m	$2 \sin \phi/(1 - \sin \phi)$
r, θ	polar coordinate system
r_1, r_2	radii defining the range of ice cover (see Fig. 1)
θ_w	half the angle of coverging boundaries (see Fig. 1)
u, v	radial and tangential velocity components
u_0, u_2	functions of r, see eq A12
x, y	Cartesian coordinate system
A, B	constants of integration
A_r	area of ice released
N_{rr}, $N_{\theta\theta}$, $N_{r\theta}$	components of stress resultants in the ice cover (N/m)
p	$-(N_{rr} + N_{\theta\theta})/2$ (N/m)
N_{nn}, N_{nt}	components of stress resultants at the boundary, see Fig. 5
N_{ij}	stress resultant in the ice cover
N_1, N_2	principal stress resultants
N_a	unconfined compressive strength of an ice cover (as defined in Fig. 2a and b)
N_b	stress resultant (defined in Fig 2a and b)
N^*	critical compressive strength of an ice cover which creates ridging and rafting in the ice cover and ice pileup on the shores
α, β	angles of ICS (defined in Fig. 10)
δ	angle of friction between ice cover and boundary
ϕ	angle of internal friction
Φ	angle defining the wind direction (see Fig. 10)
τ	wind shear stress (N/m^2)
λ	length scaling factor
ψ	angle between a radial line and larger principal stress resultant
ψ_w	value of ψ at the boundary
σ	$p + c \cot \phi$
σ_0, σ_2	functions of r (see eq A13)

MODEL STUDY OF PORT HURON ICE CONTROL STRUCTURE
Wind stress simulation

D.S. Sodhi, D.J. Calkins and D.S. Deck

INTRODUCTION

One function of an ice control structure (ICS) is to intercept individual ice floes in the early winter and retain them to facilitate formation of a consolidated ice cover. The ICS to be installed at Port Huron, Michigan, will serve such a purpose, forming a consolidated ice cover across the converging shores of Lake Huron. Already these shores provide support for an ice arch at Port Huron and hold the ice back under the present conditions even without an ICS. However, the naturally formed ice arch may break due to the anticipated increase in winter navigation, resulting in a considerable quantity of ice passing into the St. Clair River and possibly resulting in ice jams in its lower reach. The proposed ICS will have an opening to allow ships to transit, but the opening will be small to minimize the quantity of ice going into the river.

The ice cover near Port Huron consists of small floes during the periods of freezeup and breakup of the ice and a consolidated ice cover for the rest of the winter. In midwinter, winds from the south sometimes blow the ice cover to the north, where the ice is broken up by the wave action; reversal of wind direction returns the ice to the Port Huron area in an unconsolidated state. For our experiments an unconsolidated ice cover was chosen as it is considered to be more critical in terms of loading the ICS and releasing ice through the opening. Perham (1975) reported, from force data taken on an ice boom in the Beauharnois Canal, that force levels were high during the freezeup and breakup periods and low during midwinter, when the ice cover was fully consolidated from shore to shore.

The model study described in this report was designed to investigate the force interaction of an unconsolidated ice cover with the shorelines and the ICS at Port Huron, and also to determine the area of ice released during ship transits. An experimental basin was built in which the uniform wind shear stress on an ice cover was simulated by water flow beneath the ice. The forces along the boundary segments of the basin and the ICS were measured for different directions of surface shear and for different configurations of the ICS.

This report presents a theoretical model for determining the distribution of stresses along the converging boundaries of the region. This theoretical distribution is compared with the experimental results, which are presented in dimensionless form. Wind data (speed and direction) at Port Huron are summarized for the years 1976-80, and estimates are given of the possible forces on the ICS due to wind stresses and the ice release through the opening.

THEORETICAL MODELS

An unconsolidated ice cover consisting of a large number of ice floes can be treated as a continuum, provided the element length of the continuum is large compared to the typical floe size and small compared to the scales of the driving forces and the area under investigation. In the Arctic, a continuum element length scale on the order of 100 km has been adopted in most of ice dynamic models (Coon 1980, Hibler 1980) because floe sizes rarely exceed 10 km and atmospheric pressure systems are typically 1000 to 2000 km across. The ratio of the element length scale to the average floe size is taken to be approximately 1:10 in the modeling of ice drift in the Arctic.

The mass, velocity and forces of the ice for these continuum models are representative averages over a region large enough to contain many ice floes. In the following, the stress in the ice cover is represented by the stress resultant (N/m), which is obtained by integrating the stress across the thickness and averaging the stress resultant over an element length. The usefulness of a continuum approach in the analysis of the stress field in the ice cover near Port Huron will depend on the size of ice floes relative to the size of the ice cover area. The continuum approach is justified during freezeup and breakup periods as the region contains a large number of floes. Rigid-plastic models, similar to the models for granular material, have been proposed for a broken-up ice cover (Pariset and Hauser 1961, Michel 1971, Sodhi 1977, and Reimer et al. 1979).

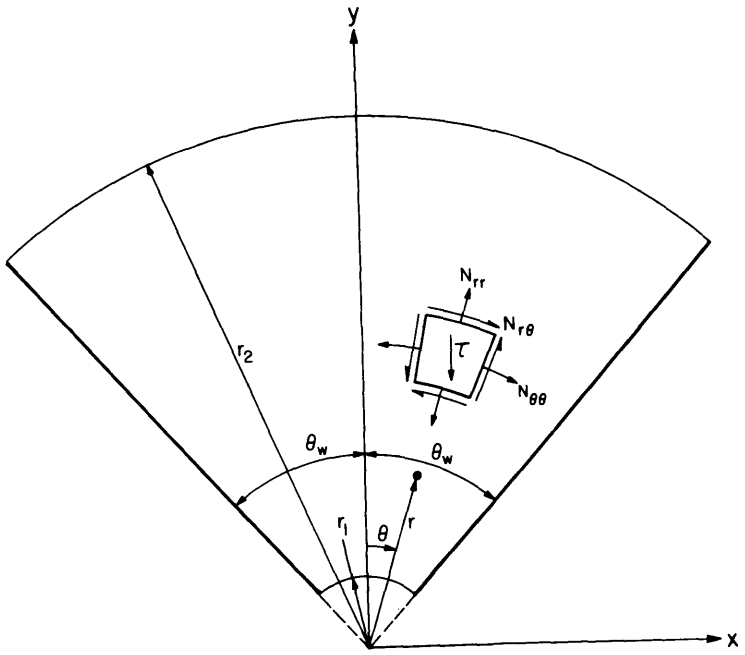

Figure 1. Geometry of an ice cover held between converging boundaries under the action of wind stress τ. The coordinate system is represented by (x, y) or (r, θ). The region of the ice cover is given $r_1 \leq r \leq r_2$ and $-\theta_w \leq \theta \leq \theta_w$. The components of the stress resultants are given by N_{rr}, $N_{\theta\theta}$ and $N_{r\theta}$.

This study is not concerned with the ice transport in the lake. Rumer et al. (1979) have presented a general summary of available information on ice transport in the Great Lakes. The present study deals with a stationary ice cover confined against the shorelines by the wind, though small-scale movement and deformation in the form of ridging and rafting within the ice cover are possible

Figure 1 shows the geometry of an unconsolidated ice cover being contained in the region of the converging shorelines and acted upon by a uniform wind stress τ. An analogy can be made between this problem and that of the flow and arching of granular material in a two-dimensional wedge-shaped hopper. The analogy exists due to similarities in 1) the ice floes and grains of the granular material, 2) the similar geometries of the Port Huron shorelines and a converging hopper, and 3) the uniform shear in the ice cover and the specific weight of the granular material. Despite of these similarities, the behavior of an ice cover and that of a confined granular material have several differences as discussed below.

The critical condition in the granular material is usually described by a Mohr-Coulomb yield criterion which is characterized by two parameters: cohesive strength (c) and the angle of internal friction (ϕ). In addition, it is implicitly assumed that the deformation of the material is in shear in a plane, i.e. in plane strain deformation. Sodhi (1977) applied this model to the arching and drift of pack ice in a wedge-shaped channel and derived an expression for the critical wind stress needed to cause movement of ice in the channel. Verification of the usefulness of the model was attempted by making comparisons with ice deformation patterns as observed with satellite imagery in the Bering Strait region and in the Amundsen Gulf.

In a similar study, Pritchard et al. (1979) use a modified yield criterion with the basic characteristics of a Mohr-Coulomb yield criterion. In the modified yield criterion, the stress resultants are always negative and of more than a certain minimum value ($-N^*$). These modifications in the yield surface are justified because an ice cover composed of a group of ice floes cannot support any tensile stress and an ice cover can resist only a certain maximum level of compressive stress resultant ($-N^*$), beyond which it deforms by ridging, rafting, shore pileup or rideup.

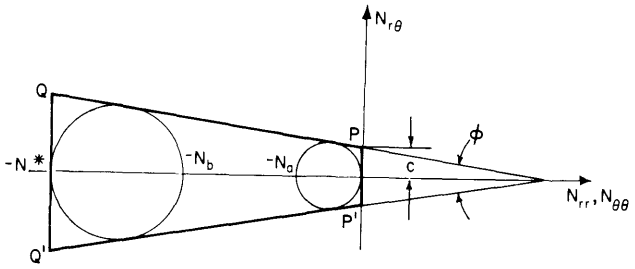

a. Mohr circle representation.

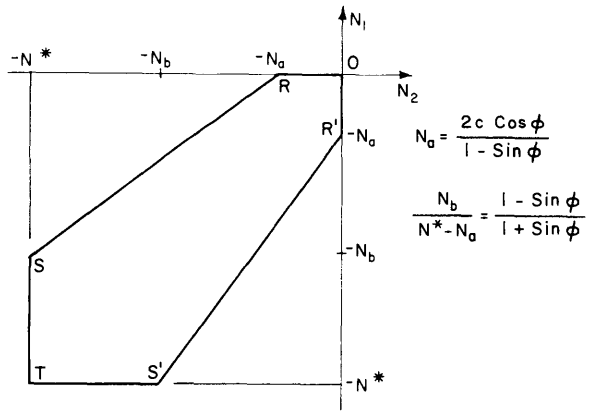

b. Principal stress representation.

Figure 2. Yield surface of an unconsolidated ice cover.

In our analysis, the yield criterion for an unconsolidated ice cover is assumed to be that used by Pritchard et al. (1979). It is depicted by a Mohr circle envelope in Figure 2a and by a yield surface in Figure 2b. The line *PQ* of Figure 2a may be defined by the following equation:

$$(N_{rr} + N_{\theta\theta}) \sin\phi - \left\{(N_{rr} - N_{\theta\theta})^2 + 4N_{r\theta}^2\right\}^{1/2} = 2c \cos\phi$$

where $-N^* \leq N_{rr} \leq 0$ and $-N^* \leq N_{\theta\theta} \leq 0$. If the state of stress point in the domain is such that the Mohr circle is tangent to line *PQ*, the deformation is in the shearing mode and equivalent to the principal stresses being represented by a point on line *RS* or *R'S'* of Figure 2b. When the Mohr circle is tangent to line *QQ'*, the deformation is in the compressional mode and equivalent to the state of stress on lines *ST* or *TS'* of Figure 2a. The state of stress represented by a point on lines *OR* or *OR'* of Figure 2b is equivalent to the Mohr circle being tangent to line *PP'* of Figure 2a. Point *R* in Figure 2b is equivalent to the unconfined compressive strength ($-N_a$), which is an important parameter related to the cohesive strength *c* of the material, as given in Figure 2.

In the plastic analysis, the state of stress is restricted to lying within or on the yield surface. To find the critical state of an ice cover, one seeks a case in which the stress in some region lies on the yield surface, and in order to simplify the analysis, we will consider a case in which the whole region lies on the yield surface. The analysis must be carried out by considering the different cases in which the state of stress lies on the three individual parts of the yield curve, i.e. lines *OR*, *RS* and *ST* of Figure 2b.

Case 1

For the case in which the stress resultants in the ice cover lie on line *RS* of Figure 2b, an analysis of the stress resultants and the velocities in the ice cover is given in Appendix A. The distribution of stress resultants along the boundary of the converging region is also derived in Appendix A for a particular set of boundary conditions, and this distribution is compared with the experimental results.

Case 2

When the stress resultants lie on line *OR* of the yield surface of Figure 2b, Reimer et al. (1979) have shown that only materials with nonzero unconfined compressive strength can form an arch to withstand the uniform wind stress and other external loads on the arch.

Case 3

For the case in which the ice is contained in a region either by an ice control structure or a natural ice arch, it is possible for the stresses in the ice cover to be in such a state that there is ridging, rafting, and shore ice piling. In such a situation, the state of stress in the ice cover is represented by points on *ST* of Figure 2b, signifying that the deformation in the ice cover would tend to make N_2 (the circumferential stress component) numerically greater than N_1 (the radial stress component). The expressions of N_2 and N_1 can be derived in terms of the wind stress τ and the limiting compressive stress N^* as proposed by Reimer et al. (1979). In a favorable situation, the deformation in the ice cover would induce an arch to form across the converging shorelines, creating shore pileups and a rubble field relieving the ice pressure on the ICS. In the worst situation, it is possible that the ICS would be loaded by the limiting compressive stress resultant N^* for the ice cover.

Though several theoretical studies have been conducted to determine the value of N^* for ridging, rafting and shore pileups, no experimental study has been conducted to verify the theoretical results. Since N^* depends upon such processes as ridging, rafting, ice pileups on shores and instability of ice blocks, it is difficult to determine its value for a given ice cover, but Prichard et al. (1979) have used a value of 1.5×10^5 N m^{-1} for N* in their analysis of sea ice flow through straits.

EXPERIMENTAL PROGRAM

Experimental facility

The simulation of wind stress on the ice cover over a large hydraulic (Froude) model area is difficult, because of the problems of blowing air uniformly over a large area and of maintaining a velocity gradient in the boundary layer to impart the required magnitude of shear stress on the ice cover. Since these difficulties could not be overcome, it was proposed that a wind stress simulation model should be constructed separately from the hydraulic model. In this model, a uniform shear stress on the floating ice cover is imparted by flowing water beneath the ice instead of blowing air over it.

A large basin, approximately 15.2 x 15.9 m (50 x 52 ft), was constructed of wood and sealed with fiberglass resin. The water level was controlled with a gate at the downstream end of the model. The basin could handle 0.34 m^3/s (12 ft^3/s), of water, which resulted in a water velocity of 0.15 m/s (0.5 ft/s) at a depth of about 0.14 m (0.46 ft). The velocity of the water could be increased by maintaining a lower water depth in the basin, but this resulted in instability and underturning of ice floes. Usually a flow rate of 0.32 m^3/s (11.3 ft^3/s) was maintained to have a depth of 0.18 m (0.58 ft) and an average water velocity of 0.11 m/s (0.37 ft/s) under the ice cover.

Figure 3 shows the general layout of the basin area and the boundary elements which skimmed the water surface from above and held back the model ice from drifting downstream. The 0.5-m-long boundary elements were attached to instrumented rods hung from a square aluminum support beam. A photograph of the boundary elements, instrumented rods and support beams is shown in Figure 4. The 6-m- (19.7-ft-) long unit, containing 12 boundary elements, could be placed at different locations relative to the direction of water flow to simulate wind from different directions.

The instrumented rods, capable of measuring forces in two directions, were connected to a data acquisition system controlled by a computer. The data acquisition system was housed in a temperature-controlled box. The instrumented rods were calibrated individually and the calibration matrices of all rods were stored on a tape. At the time of taking the force measurements, 98 channels were scanned simultaneously, with the readings transformed to force data and the averages of eight readings recorded.

Although the force measurement system had a resolution of 0.01 N, the system was sensitive to temperature variations. Considerable care had to be taken to ensure that there was little or no drift in the force measurements. Initial and final readings at the beginning and end of the experiments were compared to determine if zero drift had occurred in the force measurement.

Three types of model ice were used: 1) polyethylene plastic pieces 10 x 10 x 0.6 cm (4 x 4 x 1/4 in.), 2) freshwater ice (randomly shaped ice floes), and 3) urea ice (randomly shaped ice floes). The freshwater or urea ice sheet was grown in still water, and it was broken up to form a field of floes of random shape and given average size. After breaking the ice sheet, the water flow in the basin was started, and the water level was adjusted to the level of the boundary elements which skimmed the water surface and kept the ice in the region upstream of them. The ice

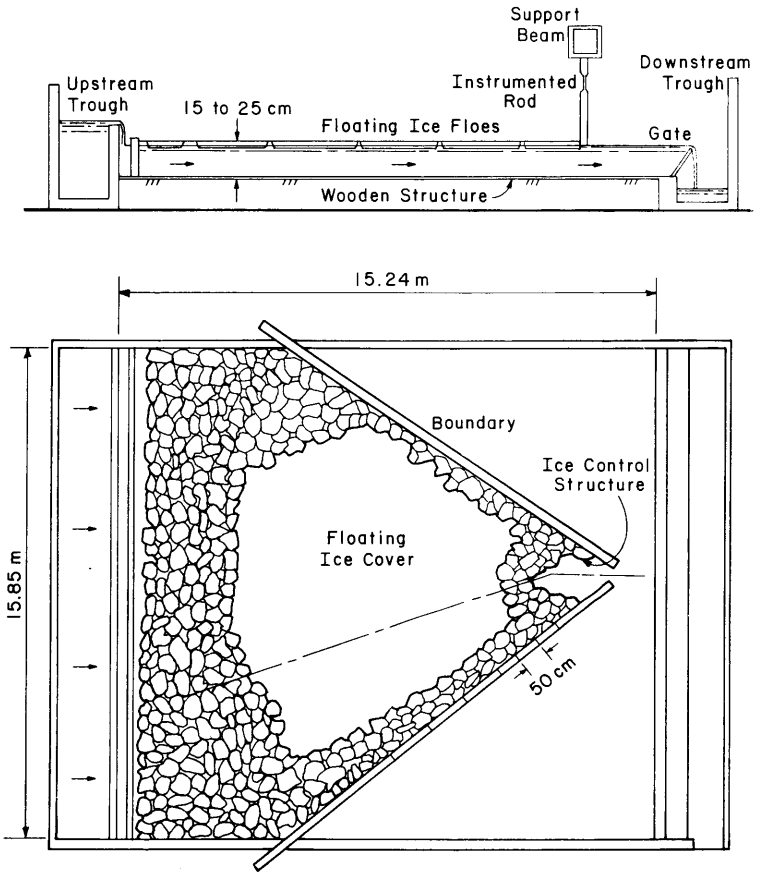

Figure 3. Sketch of the test basin.

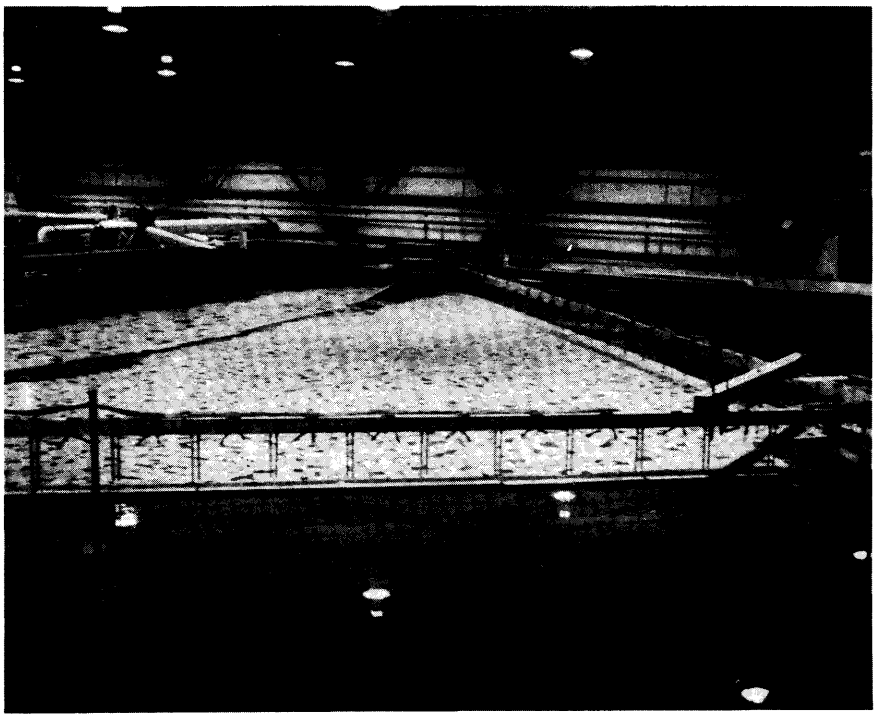

Figure 4. Photograph of the test basin.

downstream from the boundary elements was allowed to flow over the gate into the storage tank where it melted and kept the water temperature close to 0°C.

The shear stress imparted by the water to the model ice cover was determined by summing the measured force components in the streamwise direction. The total force was then divided by the area of the cover to obtain the uniform shear stress τ acting on the ice cover.

Scaling factors

In order to relate model results to prototype values, the experimental results are presented in a nondimensional form that can be used for both the model and the prototype. The expressions derived for the stress resultants in Appendix A have been normalized with respect to the product of shear stress τ and the distance d of the ice cover region shown in Figure 5. For the corresponding points in the prototype and the model, the normalized stress components are functions of the position of the point, provided the behavior of the broken-up model ice cover represents the prototype behavior. Referring to Figure 5, we have

$$\left(\frac{N_{ij}}{\tau d}\right)_{prototype} = \left(\frac{N_{ij}}{\tau d}\right)_{model} = f(\text{position of a point}).$$

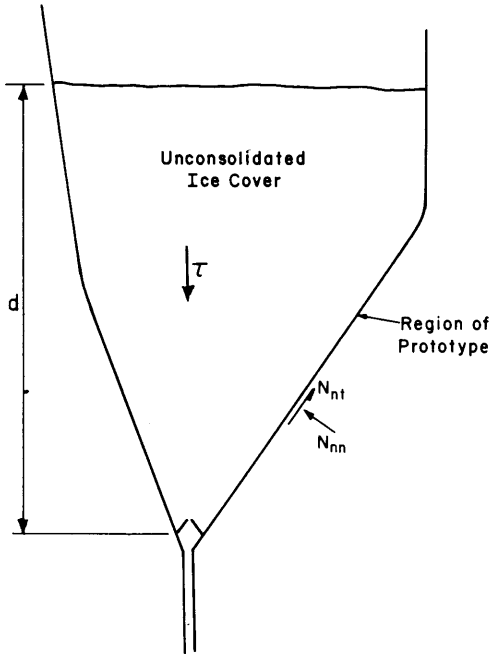

Figure 5. Scale factors for the wind stress simulation.

One can use the above equation for the prototype condition in the following manner:

$$(N_{ij})_{prototype} = (\tau d)_{prototype}\left(\frac{N_{ij}}{\tau d}\right)_{model}.$$

The distribution of normalized stress $(N_{ij}/\tau d)$ is determined from model experiments. The factor (τd) for the prototype is estimated from the wind data and the extent of the ice cover.

Experimental results

The results of the experiments are presented in three categories: 1) distribution of stress components along the converging boundaries without an ICS, 2) normalized loads for various configurations of the ICS and 3) the area of ice released during ship transits.

Distribution of stress components along the converging boundaries

The region of the floating ice cover for these experiments is shown in Figure 1. The included angle between the boundaries is 84°, approximately the angle between the shore-fast ice edges at Port Huron. The direction of the uniform shear stress is parallel to the line of symmetry of the region. Both plastic pieces and freshwater ice were used in the experiments to determine any significant differences in their behavior.

The main reason for conducting this set of experiments was to verify the theoretical distribution of normal stress resultants along the boundary as given by eq A26. The experiments were conducted so that the ice cover would move upstream a small distance from the boundaries. Then it would travel forward and come to rest against the boundary elements after deformation took place within the ice cover, due to the interaction of ice with the boundaries. The deformation was equivalent to creating a critical state of stress in the ice cover, and the distribution of stress along the boundary was fixed once the ice cover stopped moving.

Figure 6a is a plot, divided into 0.5-m-long boundary segments, of the typical force measurement across the basin in the normal and tangential directions relative to the boundary. The distribution of the stress components shows a trend, but there is considerable variation from segment to segment. This variation results from the measuring elements not being long enough compared to the floe size to give an average representative value of the stress resultant. When the same data are plotted in Figure 6b by summing stress resultants over 1-m-long boundary segments, the trend of representative stress resultants

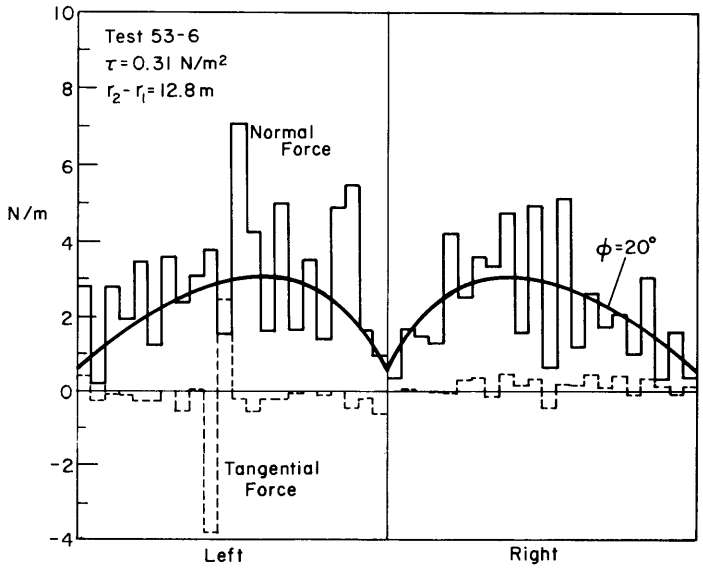

a. Measuring element length = 0.5 m, freshwater ice floes used.

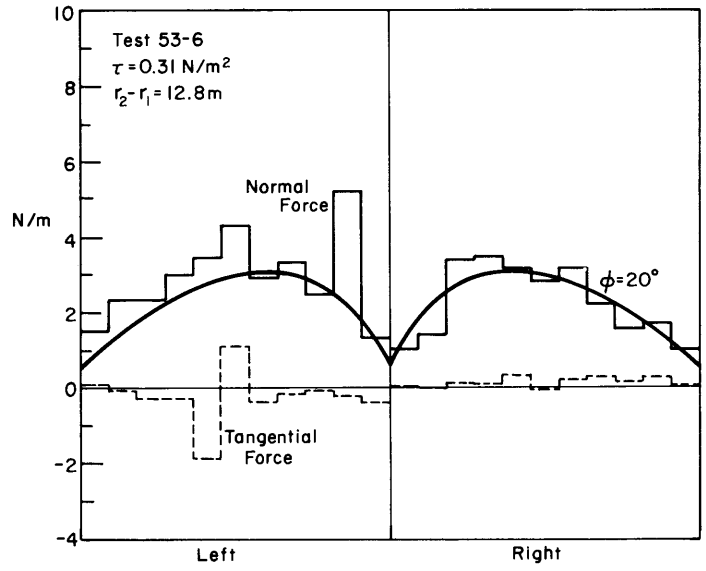

b. Same as in Figure 6a, but measuring element length = 1 m.

Figure 6. Distribution of measured boundary stress in the normal and tangential directions and the theoretical distribution of normal stresses (eq A26, ϕ = 20°).

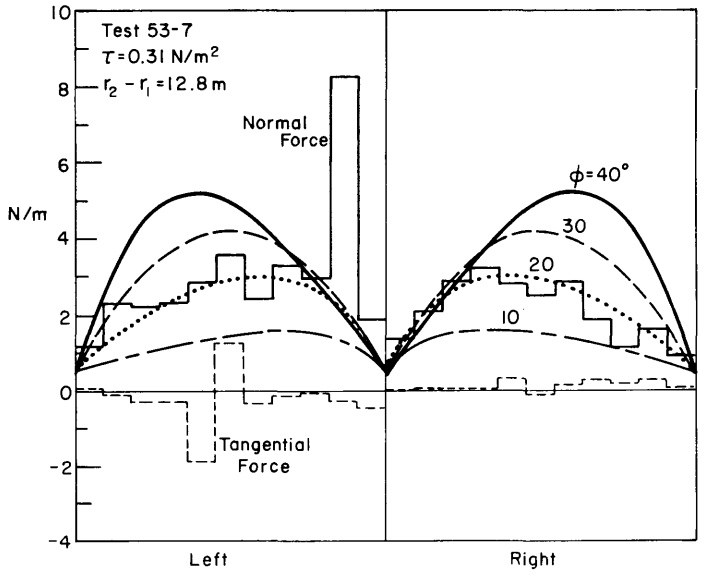

Figure 7. Same data presentation as in Figure 6b for a reading taken 4 minutes later. Theoretical distribution of $N_{\theta\theta}$ (eq A26) is plotted for $\phi = 20°, 30°, 40°$.

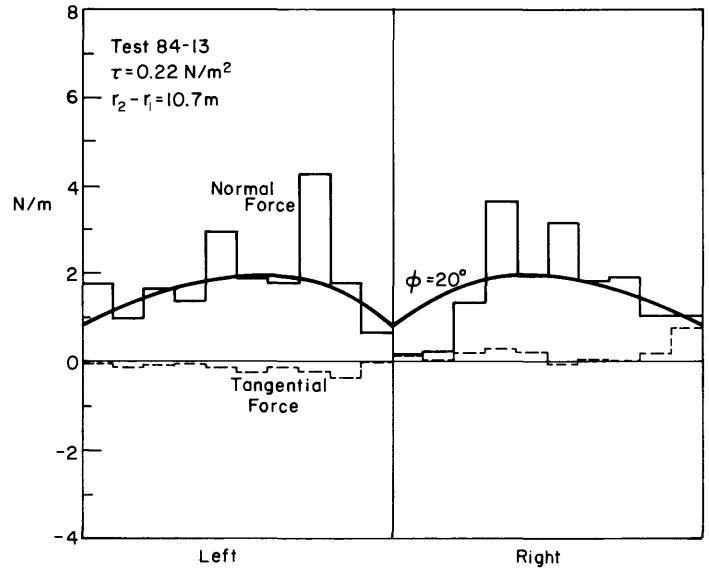

Figure 8. Same data presentation as in Figure 6b for different test conditions.

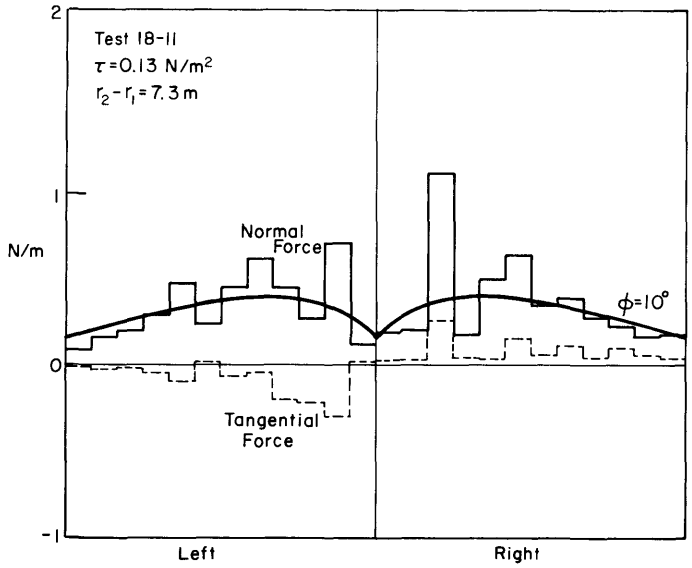

Figure 9. Same data presentation as in Figure 6b for polyethylene pieces (10 x 10 x 0.6 cm).

can be easily seen. Figure 7 shows the same type of plot as Figure 6b but for a force measurement taken 4 minutes later. The ratio of the measuring length of (1 m) to the average floe size (10 cm) is approximately 10, a ratio used in many problems that are concerned with flow in granular media.

The theoretical distribution of stress resultants at the boundary is given in eq A26 for a frictionless boundary condition. The measured tangential forces along the boundary are low, and thus comparison of the theoretical and experimental distributions of the normal stress resultant at the boundary is justified. Figures 6 and 7 also show the distribution of normal stress components at the boundary as given by eq A26. Similar distributions of theoretical and measured normal stress components are presented in Figures 8 and 9 for freshwater and polyethylene pieces, respectively.

The similarity between the theoretical and measured distribution of the normal stress resultant is good except at a few points. From these comparisons, it is deduced that a fragmented ice cover can be modeled with a Mohr-Coulomb yield surface and that the angle of internal friction is about 20° for freshwater ice and is about 10° for plastic pieces.

Forces on the ice control structure

Experiments were conducted to determine the forces exerted by the ice cover on the ICS, which was attached to transducer rods at the downstream end of the ice cover as shown in Figure 10. The measured forces on each end of the ICS were added to determine the force per unit length of the ICS, which was then normalized by τd (see Fig. 10).

For each test, a particular configuration of the ICS was chosen, and the force measurements were taken after disturbing the ice cover. This procedure was repeated several times during the course of a test, and the average normalized forces per unit length of the ICS were computed for each test. These average values for all the tests are presented in Tables 1 and 2 for plastic pieces and freshwater ice, respectively.

Many problems were encountered during measurement of forces due to humidity and temperature variations in the instrument box. The results of the ice force tests do not indicate clearly any particular pattern, but the following two conclusions may be made with caution:

1. As the distance from the apex to the ICS (distance e in Fig. 10) decreases, the ICS seems to move progressively under the protection of an arch, and thus experiences smaller forces from the ice cover.
2. The orientation of the ICS affects the force transmitted to it by assisting in the formation of an ice arch across the converging boundaries.

As mentioned earlier, these conclusions are not clearly indicated by the results of the small number of tests, but there is a trend towards them in the

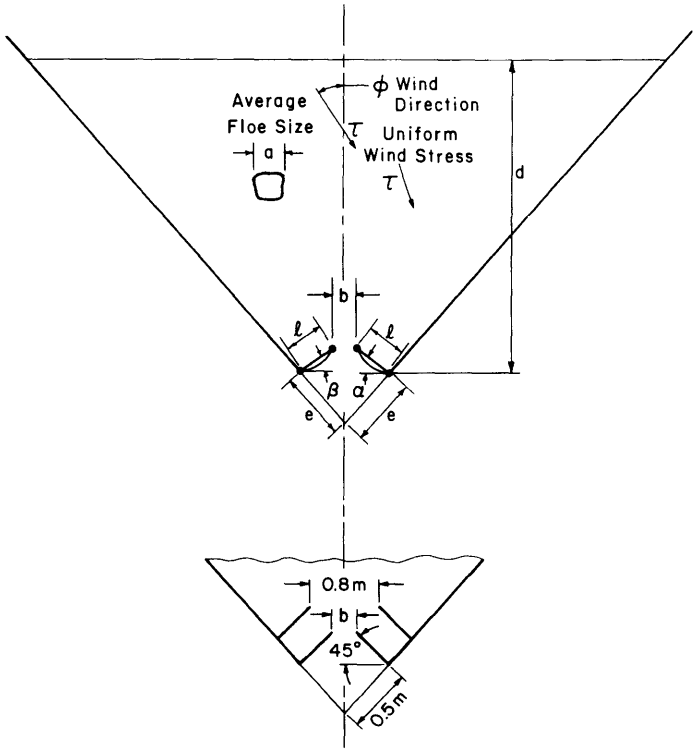

Figure 10. Geometry of an ice control structure for force and ice release measurements.

Table 1. Average normalized total force per unit length of the ice control structure when using polyethylene pieces (10 x 10 x 0.6 cm).

Experiment	α, β	e *(m)*	ℓ *(m)*	*Average value of* N/τd
11	0°	1.10	0.60	0.98
12	23°	1.10	0.70	0.95
13	51°	1.10	1.00	0.69
15	0°	2.00	1.20	0.85
16	0°	1.10	0.60	1.23
18	0°	0.76	0.30	0.71

Table 2. Average normalized total force per unit length of the ice control structure when using freshwater ice.

Experiment	α, β	e *(m)*	ℓ *(m)*	*Average value of* N/τd
60	34°	3.65	2.74	1.16
61	34°	3.65	2.74	1.15
62	0°	3.65	1.83	2.22
63	-30°	3.65	2.59	0.31
64	-30°	3.65	2.59	0.67
65	36°	3.65	2.44	–
66	36°	3.65	2.44	2.57
67	36°	3.65	2.44	2.52
68	36°	3.65	2.44	1.76
69	45°	1.98	1.37	1.46
70	0°	1.98	1.22	0.63
71	0°	1.98	1.22	1.94
72	0°	1.98	1.22	0.82
73	0°	1.98	1.22	0.62
74	-36°	1.98	1.52	0.71
75	45°	1.98	1.37	1.29
76	45°	1.98	1.37	–
77	70°	1.98	1.52	1.26

results. More comments will be made on these results in the *Summary and Conclusions.*

Area of ice released during ship transits

Experiments were conducted to measure the area of ice released through the opening in the ICS when the ice cover was disturbed by moving a blunt object, representing ship transits through the ice cover. The tests were conducted for different orientations (α, β) and positions of the ICS (*e*) and for different sizes of the opening (see Fig. 10). These tests were conducted using plastic pieces and broken-up freshwater and urea ice. The average flow size *a* was determined by weighing a number of floes. The area of ice released during each ship transit was determined by weighing the ice. The area of ice was then normalized with respect to the square of the opening in the ICS, and the mean value of the normalized area of ice released was determined for 20

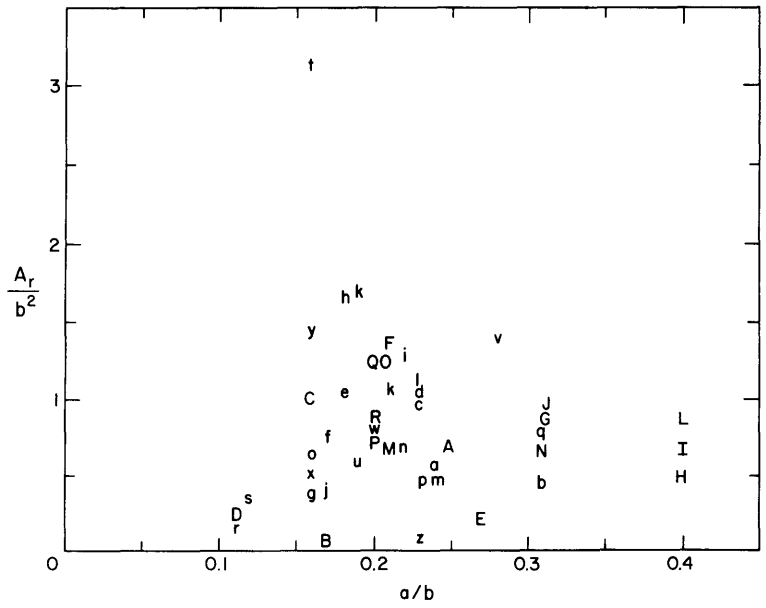

Figure 11. Plot of mean normalized ice discharge A_r/b^2 *with respect to* a/b *for upbound ship passages.*

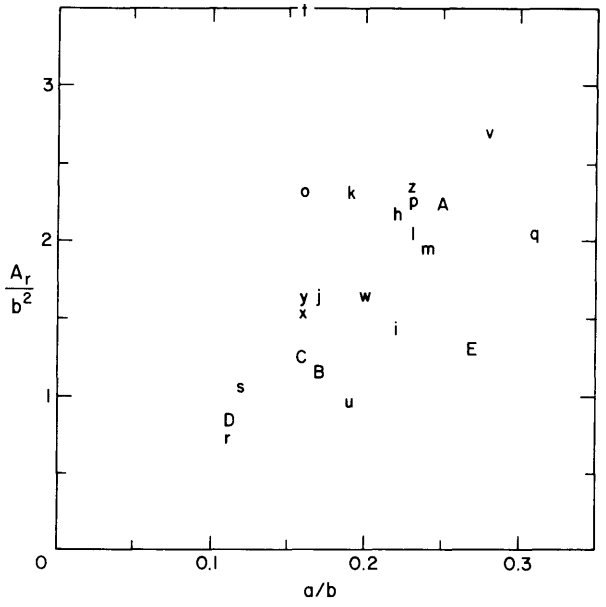

Figure 12. Plot of mean normalized ice discharge A_r/b^2 *with respect to* a/b *for downbound ship passages.*

upbound and 20 downbound passages of ship. The ice release during the ship transits was a random phenomenon that depended upon the arrangement of ice floes near the opening before the occurrence of arching. The ability to arch has been demonstrated to be a function of *b/a* by Calkins and Ashton (1975).

The mean normalized ice area released (A_r/b^2) during ice release experiments is plotted with respect to the ratio of the average floe size to the opening in the ICS (a/b) in Figures 11 and 12 for the upbound and downbound ship passages, respectively. The symbols in Figures 11 and 12 refer to the results of a particular test conducted for a particular configuration of the ICS. The details of each particular test are given in Table 3.

No definite trend can be seen in the results of these tests since the data are so scattered. The values of mean normalized ice area released are higher than those obtained from the tests conducted in the hydraulic model (Calkins et al. in prep). This increase is perhaps attributable to high values of shear stress τ acting on the ice cover, as they are an order of magnitude higher than those for the tests conducted in the hydraulic model. The only conclusions that can be reached are that 1) the ice cover arches for low values of a/b (0.11), and 2) the mean values of normalized ice area released (A_r/b^2) are less than 3 for downbound ship passages and less than 2 for upbound ship passages, with the exception of the data from one particular test.

The results of the ice release data (Table 3) indicate less release of ice when the wind is blowing from a direction other than along the centerline. The decrease in ice release is associated with the oblique incidence of the opening in the ICS relative to the ice floe movement.

Table 3. Results of ice release experiments*.

Experiment number	Type of ice†	Orientation of ICS α, β	Distance from apex e (m)	Floe size a (mm)	Size of opening b (cm)	Ice thickness t (mm)	Symbol††	Ratio of floe to opening a/b	Ice release A_r/b^2 Upbound	Ice release A_r/b^2 Downbound	Wind Direction ϕ
60	W	34°	3.65	123	51	-	a	0.24	0.54	-	0°
61	W	34°	3.65	159	51	-	b	0.31	0.43	-	0°
62	W	0°	3.65	115	51	11	c	0.23	0.98	-	0°
63	W	-30°	3.65	119	51	15	d	0.23	1.04	-	0°
64	W	-38°	3.65	92	51	30	e	0.18	1.03	-	0°
65	W	36°	3.65	86	51	18	f	0.17	0.76	-	0°
66	W	36°	3.65	80	51	11	g	0.16	0.39	-	0°
67	W	36°	3.65	91	51	9	h	0.18	1.56	-	0°
68	W	36°	3.65	113	51	25	i	0.22	1.29	1.46	0°
69	W	45°	1.98	88	51	13	j	0.17	0.40	1.63	0°
70	W	0°	1.98	97	51	23	k	0.19	1.67	2.31	0°
71	W	0°	1.98	116	51	26	l	0.23	1.08	2.05	0°
72	W	0°	1.98	122	51	14	m	0.24	0.47	1.96	0°
73	W	0°	1.98	110	51	13	n	0.22	0.68	2.17	0°
74	W	-36°	1.98	83	51	15	o	0.16	0.6	2.3	0°
75	W	45°	1.98	79	34	13	p	0.23	0.47	2.28	0°
76	W	45°	1.98	75	24	9	q	0.31	0.78	2.04	0°
77	W	45°	1.98	87	80	13	r	0.11	0.14	0.72	0°
78	U	45°	1.98	96	80	12	s	0.12	0.31	1.05	0°
79	U	45°	1.98	83	51	21	t	0.16	3.14	3.51	0°
80	W	45°	1.98	95	51	15	u	0.19	0.58	0.97	0°
81	W	45°	**	113	41	15	v	0.28	1.38	2.70	0°
82	W	45°	**	82	41	26	w	0.20	0.69	1.63	0°
83	W	45°	**	117	51	18	x	0.16	0.49	1.55	0°
90	W	45°	1.98	100	61	20	y	0.16	1.42	1.61	21°
91	W	45°	1.98	94	41	19	z	0.23	0.08	2.33	21°
92	W	45°	1.98	126	51	23	A	0.25	0.69	2.26	21°
93	W	45°	1.98	89	51	25	B	0.17	0.05	1.17	42°
94	W	45°	1.98	95	61	25	C	0.16	0.50	1.28	42°
95	W	45°	1.98	93	81	24	D	0.11	0.23	0.86	42°
96	W	45°	1.98	217	81	25	E	0.27	0.20	1.30	42°
27	P	45°	4.00	100	48	6	F	0.21	1.13	-	0°
29	P	45°	4.00	100	33	6	G	0.31	0.84	-	0°
30	P	45°	4.00	100	25	6	H	0.40	0.48	-	0°
31	P	0°	4.00	100	25	6	I	0.40	0.6	-	0°
32	P	0°	4.00	100	33	6	J	0.31	0.86	-	0°
33	P	0°	4.00	100	48	6	K	0.21	1.02	-	0°
34	P	-30°	4.00	100	48	6	L	0.40	0.84	-	0°
40	P	-30°	4.00	100	33	6	M	0.21	0.64	-	0°
41	P	-30°	4.00	100	25	6	N	0.31	0.64	-	0°
43	P	45°	4.00	100	48	6	O	0.21	1.24	-	0°
45	P***	45°	4.00	200	102	6	P	0.20	0.72	-	0°
113	P	45°	4.00	100	51	6	Q	0.20	1.26	-	30°
114	P	45°	4.00	100	51	6	R	0.20	0.80	-	45°

* Refer to Figure 10 for the interpretation of each letter listed in this table.
† W—freshwater ice, P—plastic pieces, U—urea ice.
** Double booms were used for these tests as shown in Figure 10.
†† The following symbols are used to plot the results in Figures 11 and 12.
*** Randomly shaped plastic pieces.

ANALYSIS OF WIND DATA FOR LOWER LAKE HURON

The data on wind conditions in the study area were obtained from three sources. The U.S. Army Detroit District, Corps of Engineers received a wind analysis for January, February and March, for Sarnia, Ontario (from Acres American Inc. 1974). The National Oceanic and Atmospheric Administration (NOAA) published a regional set of meteorological parameters for Southern Lake Huron for 1960–73, but this summary omits January through March. The third data set comes from the U.S. Coast Guard Station at Port Huron, and is on file for the years 1975–1980.

The Acres American Inc. (1974) study showed that the mean maximum hourly wind speed was roughly 20 mph from all eight quadrants. The maximum wind speed was 39 mph from the SW quadrant, and this was defined as the maximum one-hour value. The NOAA data indicated that, for the 0.1% event between 1960–73, the wind speed was greater than 48 mph, but only for those nine months indicated in Table 4.

Table 4 . Summary of wind data (Acres American, Inc. 1974 and NOAA 1960-73).

Wind direction	Mean wind speed (mph) Jan-Mar (1960-66) Acres	Mean wind speed (mph) Apr-Dec (1960-73) NOAA	Frequency (%) Apr-Dec	Frequency (%) Jan-Mar	Maximum wind speed Jan-Mar (mph)
N	11.7	16.4	12.2	5	32
NE	10.4	14.7	9.8	9	25
E	9.0	13.4	8.1	7	29
SE	10.8	14.0	11.6	15	33
S	10.1	15.1	16.0	11	30
SW	11.6	15.9	15.2	16	39
W	10.8	16.9	14.6	19	36
NW	11.6	16.1	11.8	18	33

Table 5. Fort Gratiot maximum recorded wind velocities (mph) (maximum 3-hr velocity/direction).

	1974-75	1975-76	1976-77	1977-78	1978-79	1979-80
Dec	-	-	32/SW	37/NE	30/SW	30/SW
Jan	35/S	27/N	28/NE	30/NE	27/N	35/SE
Feb	30/SW	30/E	25/NW	27/N	20/NW*	33/N
Mar	30/E	25/SW	40/NW	26/N	30/SE	40/SW

*Partial record for that month.

The frequency of duration is obviously different depending upon the months considered. The data in Table 4 show that the wind direction has a preferred SW to NW pattern during the winter months. The wind direction is uniformly distributed during the other nine months. The mean wind speed is slightly higher for the nonwinter months.

Data from the Fort Gratiot Coast Guard Station at Port Huron have been reported for 6-hr quarters with the basic data collected at 3-hr intervals. The Detroit District abstracted the information from their files to a computer base file. The data given in Table 5 are abstracted from the basic data and represent the maximum monthly 3-hr wind velocity. Table 5 summarizes the frequency of wind duration for the five years on the monthly basis. The months of January and February show a strong SW to NW pattern of wind direction while March has a more balanced pattern. The monthly summaries for five years (1976-80) are given in Appendix B. A maximum wind speed of 30 to 40 mph occurs occasionally. Winds of shorter duration, but higher speed, have probably not been included in these records. The six years of wind data from Fort Gratiot show the same general trend as that found by Acres American, Inc. (1974). The wind directions from the southwest to northwest quadrants account for more than 50% of the duration.

SUMMARY AND CONCLUSIONS

The first set of experiments was conducted to determine the distribution of stress components at the boundaries of a converging region of ice cover acted upon by wind stress, and the results are presented in nondimensional form. Hence these results can be applied to a region of any size for which the behavior of an ice cover can be represented by that in the model experiments.

In the second set of experiments, an ice control structure was installed in the model with the objective of determining the amount of ice released through the opening in the ICS and the ice forces on the ICS. In this case, a length scaling factor can be obtained from the similarity of the prototype and model geometry.

Release of ice through the opening of an ICS

Referring to Table 3 or Figures 11 and 12, we conclude that the ice cover arches for low values of $a/b \cong 0.11$ to 0.15, and that the mean average value of normalized ice area (A_r/b^2) released is less than 3.

If the average size of prototype ice floes is about 20 m (65 ft), the ice cover would arch across an 133-m- (437-ft-) wide opening in the ICS for a/b = 0.15. If the size of the opening is selected to 76 m (250 ft) and a/b = 0.15, an ice cover will arch when the average size of the floes is 11.4 m (37 ft).

Taking a figure of $A_r/b^2 = 3$, an estimate of ice release for 100 round trips of ships through an opening of 122 m (400 ft) in the ICS is approximately 9 km^2 (3.45 mile^2). This figure should be multiplied by a factor for the probability of ship transits during high winds.

Ice forces on the ice control structure

While conducting ice release experiments, we measured the ice forces on the model ICS, and the normalized ice forces per unit length of ICS are given in Table 1 and 2. From Figure 10 and the probable location of the ICS near Port Huron, a length-scaling factor can be determined by taking the ratio of distances (e) in the model and in the prototype. The approximate location of the ICS along the U.S. and the Canadian shorelines is known to be 762 m (2500 ft) uplake from the mouth of the St. Clair River. The corresponding lengths in the model are 1.98 m (6.50 ft) and 3.65 m (12 ft) (see Table 2 and Fig. 10). Thus the length scale factor λ is equal to 385 or 209, depending upon the distances (e) in the model. For the case of $\lambda = 385$, a cover length of 11.50 m (37.75 ft) in the model corresponds to 4.43 km (2.75 miles) of cover length in the prototype. This cover length is not long enough to be certain that an ice cover beyond this distance would not load the ICS more than the ice cover within this distance. A longer ice cover length could be achieved either by having a larger model area or by conducting a test with larger values of the length scale factor λ. The first approach would have meant constructing a larger test facility. The second approach has limitations in terms of conducting a test with a very small model of the ICS and even smaller ice floes. For the ice release experiments, the ice cover was sufficiently large because ice release occurs from an area adjacent to the ICS.

Despite the insufficient length of the model ice cover, it is useful to estimate the ice forces per unit length of the ICS from the force measurements taken during the ice bleeding experiments. The values of normalized total load ($N/\tau d$) on the ICS (given in Table 3) range from 0.31 to 2.52, and their average value is 1.3. The variation in these measurements is attributed to the possible problems of drift in the force-measuring system due to temperature variations, although great care was taken to avoid them. The variations may also result from different arrangements of ice floes and changes in the behavior of the ice cover. Despite the variation, the normalized force ($N/\tau d$) on the ICS is taken to be equal to 1.0 in the following discussion.

From the wind data for Port Huron, a maximum wind velocity of about 18 m/s (40 mph) is anticipated. The value of wind shear stress is estimated from the expression, $\tau = c_d \rho V^2$, in which a value of 0.003 for c_d and 1.3 kg/m^3 for ρ (density of air) is taken. Thus, $\tau = 1.26$ N/m^2 (1.83×10^{-4} psi) for a wind velocity of 18 m/s ($\approx$40 mph). For a cover length of 4.43 km (2.75 miles), we get a value of $(\tau d)_{prototype}$ = 5600 N/M (383 lbf/ft). If we assume the thickness of ice to be 0.5 m, a force of 5600 N/m (383 lbf/ft) is equivalent to 11.2 kPa (1.62 psi) in the ice cover. These values should be multiplied by a factor of 2.5 to take into account the variation of the normalized load in the experiments. This computation results in a load on the ICS equal to 14,000 N/m (959 lbf/ft) or to an ice pressure of 28 kPa (4.06 psi) for a 0.5-m-(20-in.-) thick ice cover. These estimates would be valid for ice cover lengths of up to 5 km.

Ice forces on ice control structure from a large unconsolidated ice cover

The shoreline configuration of the southern end of Lake Huron is sketched in Figure 13, and appears similar to that considered in the theoretical model. From the observations made in the field and the model experiment, we can expect that the ice cover near the ICS will be trapped between the shores of the lake and the ICS in the form of wedge-shaped zones (shown as shaded areas in Fig. 13). Probably these zones will be frozen to the shore bottom due to formation of a rubble field and grounded ridges, and in such cases any force transmitted to these zones will be transmitted to the shore. On the other hand, if these wedges are not frozen but remain unconsolidated, as would be the case in early and late winter, the ice pressure from the ice cover will result in pressure on the ICS. We make an assumption that the ice pressure on the ICS is equal to the ice pressure exerted on the stationary ice zones from the main body of the ice cover, i.e. an assumption of an isotropic state of stress in the wedge-shaped zone. This assumption is considered to be conservative.

If the shear stress acting on the ice cover is large enough to create a state of stress large enough for it to deform in its plane, a slip (or shear) line will develop between the stationary ice cover adjacent to the ICS and the main body of the ice cover. The boundaries of the main body of the ice cover are approximately straight, and we can make use of the expression developed for the distribution of normal stress components along the boundary (eq A26). As indicated by Figure 13, we have assumed that the unconsolidated ice field extends to about 50 km and the lower end of the ice cover is at 1 km from the apex of the converging boundaries. The nondimensional normal stress component, $N_{\theta\theta}/\tau(r_2-r_1)$, in

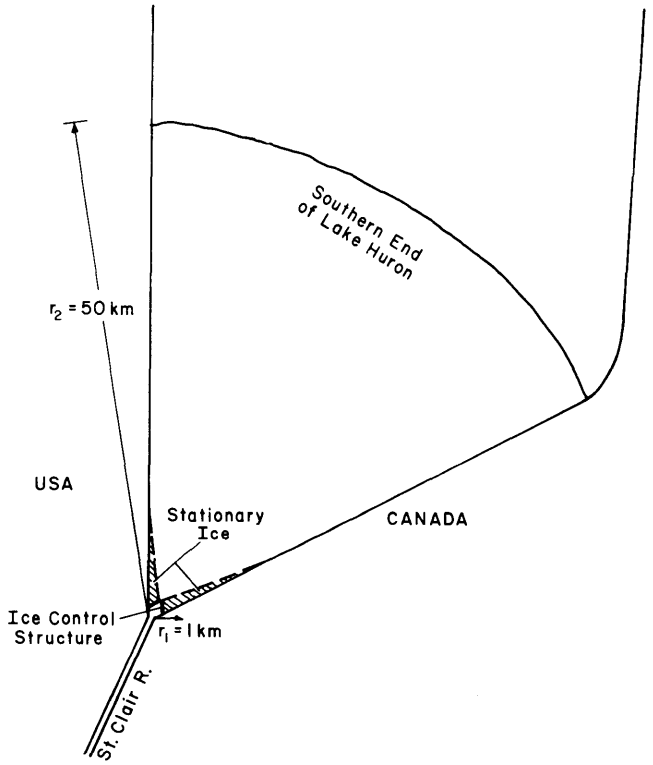

Figure 13. Sketch of southern Lake Huron.

the lower end of the ice cover is approximately equal to 0.08 (from eq A26 for an assumed value of $\phi = 20°$ and $r_2/r_1 = 50$). Therefore, $N_{\theta\theta}$ is estimated to be 5057 N/m (347 lbf/ft) for $r_2 - r_1 = 49$ km and $\tau = 1.26$ N/m^2. Making use of the assumption of an "isotropic" state of stress in the wedge-shaped zones, we estimate the force per unit length of the ICS to be approximately 5000 N/m (342 lbf/ft), which is equivalent to 10 kPa (1.45 psi) of pressure in a 0.5-m-(≈20-in.-) thick ice cover.

LITERATURE CITED

Acres American Inc. (1974) Model of the Little Rapids Cut area of the St. Marys River, Michigan. Report DACW35-73-C-0208, U.S. Army Corps of Engineers, Detroit District

Brennen, C. and J.C. Pearce (1978) Granular material flow in two dimensional hoppers. *Transactions of ASME, Journal of Applied Mechanics,* vol. 45, p. 43-50.

Calkins, D.J. and G.D. Ashton (1975) Arching of fragmented ice covers. CRREL Special Report 222, AD A009499.

Calkins, D.J., D.S. Sodhi and D.S. Deck (in prep.) Port Huron ice control model study—Hydraulic model. CRREL Report in preparation.

Coon, M.D. (1980) Review of AIDJEX modeling. *Proceedings, Symposium on Sea Ice Processes and Models* (R.S. Pritchard, Editor) Seattle: University of Washington Press.

Hibler, W.D. III (1980) A dynamic thermodynamic sea ice model. *Journal of Physical Oceanography,* vol. 9, no. 4, p. 815-846.

Michel, B. (1971) Winter regime of rivers and lakes. CRREL Monograph III-Bla, p. 83-99. AD724121.

National Oceanic and Atmospheric Administration (1975) Summary of synoptic meteorological observations for Great Lakes areas: Vol. 2. Lake Huron and Georgian Bay. National Climatic Center, Asheville, North Carolina.

Pariset, E. and R. Hauser (1961) Formation and evolution of ice covers on rivers. *Transactions of the Engineering Institute of Canada,* vol. 5, no. 1, p. 41-50.

Perham, R.E. and L. Racicot (1975) Forces on an ice boom in the Beauharnois Canal. *Proceedings of the 3rd International Association of Hydraulic Research Symposium on Ice Problems,* Hanover, New Hampshire.

Pritchard, R.S., R.W. Reimer and M.D. Coon (1979) Ice flow through straits. *Proceedings of the 5th International Conference on Port and Ocean Engineering Under Arctic Conditions*, Norwegian Institute of Technology, Trondheim, Norway, vol. III, p. 61-74.

Reimer, R.W., R.S. Pritchard and M. Coon (1979) Beaufort and Chukchi Sea ice motion, Part 2. Onset of large scale Chukchi Sea ice breakout. Flow Research Inc., Report No. 133, Kent, Washington.

Rumer, R.R., R. Crissman, A. Wake (1979) Ice transport in Great Lakes. Report prepared for Great Lakes Environmental Research Laboratory, NOAA, Ann Arbor, Michigan.

Sodhi, D.S. (1977) Ice arching and the drift of pack ice through restricted channels. CRREL Report 77-18. ADAO44218.

APPENDIX A. EQUATION FOR THE STRESS RESULTANTS AND VELOCITIES OF THE ICE COVER

The purpose of this appendix is to present the equations for the stress resultants and velocities in the ice cover when it is in a critical state (defined by the state of stress resultants on line *RS* of Fig. 2b) and to derive a solution of these equations for a particular case. The region ($r = r_1$ to r_2 and $\theta = -\theta_w$ to $+\theta_w$) of the ice cover is shown in Figure 1, and the ice is held against the boundaries by a uniform wind stress τ acting on the ice cover.

The governing equations, written in the polar coordinate system (r, θ) shown in Figure 1, are given below. In these equations u and v are velocity components along the r and θ directions.

Continuity:

$$\frac{\partial u}{\partial r} + \frac{u}{r} + \frac{1}{r}\frac{\partial v}{\partial \theta} = 0. \tag{A1}$$

Equilibrium:

$$\frac{\partial N_{rr}}{\partial r} + \frac{1}{r}\frac{\partial N_{r\theta}}{\partial \theta} + \frac{N_{rr} - N_{\theta\theta}}{r} = \tau \cos\theta \tag{A2}$$

$$\frac{\partial N_{r\theta}}{\partial r} + \frac{1}{r}\frac{\partial N_{\theta\theta}}{\partial \theta} + \frac{2N_{r\theta}}{r} = -\tau \sin\theta\,. \tag{A3}$$

Yield criterion:

$$(N_{rr} + N_{\theta\theta}) \sin\phi - \left\{(N_{rr} - N_{\theta\theta})^2 + 4N_{r\theta}^2\right\}^{1/2} = 2c\cos\phi\,. \tag{A4}$$

Isotropy:

$$\frac{2N_{r\theta}}{N_{rr} - N_{\theta\theta}} = \left(\frac{\partial v}{\partial r} - \frac{v}{r} + \frac{1}{r}\frac{\partial u}{\partial \theta}\right) \Big/ \left(2\frac{\partial u}{\partial r}\right). \tag{A5}$$

where

N_{rr}, $N_{\theta\theta}$, $N_{r\theta}$ = normal and shear components of stress resultants. These have units of force per unit length as they are the integrated stress across the thickness of the ice cover and represent the force interaction between floes across an elemental length equal to approximately 10 times the average floe size.

τ = the uniform wind stress per unit area of the ice cover directed toward the negative y axis as shown in Figure 1.

c, ϕ = cohesive strength and the angle of internal friction of the ice cover during in-plane shear deformation (see Fig. 2 for its use in defining the yield criterion).

The above five equations are to be solved for five unknown functions, u, v, N_{rr}, $N_{\theta\theta}$ and $N_{r\theta}$, which must also satisfy the boundary conditions. The solution follows a procedure similar to that of Brennen and Pearce (1978), and the present analysis focuses on the derivation of the expressions for the stress resultants along the boundary of the ice cover region. Introducing Sokolovski functions (p, ψ), we define the stress resultants in the following way such that the yield criterion is satisfied:

$$N_{rr} = -p + (p \sin\phi + c\cos\phi)\cos 2\psi$$

$$N_{\theta\theta} = -p - (p \sin\phi + c\cos\phi)\cos 2\psi$$

$$N_{r\theta} = (p \sin\phi + c\cos\theta)\sin 2\psi \tag{A6}$$

where $p = -(N_{rr} + N_{\theta\theta})/2$ and ψ is the angle between the greater principal stress and the radial direction.

Using eq A6 and introducing $\sigma = p + c \cot \phi$, we may rewrite eq A2, A3, and A5 as given below:

$$(1 - \sin\phi \cos 2\psi)\ \frac{\partial \sigma}{\partial r} + 2\sigma \sin\phi \sin 2\psi\ \frac{\partial \psi}{\partial r}$$
$$- \sin\phi\ \sin 2\psi\ \frac{1}{r}\frac{\partial \sigma}{\partial \theta} - \frac{2\sigma}{r} \sin\phi \cos 2\psi \left(\frac{\partial \psi}{\partial \theta} + 1\right) + \tau \cos\theta = 0 \qquad \text{(A7)}$$

$$(1 + \sin\phi\ \cos 2\psi)\ \frac{1}{r}\frac{\partial \sigma}{\partial \theta} - \frac{2\sigma}{r} \sin\phi\ \sin 2\psi \left(\frac{\partial \psi}{\partial r} + 1\right)$$
$$- \sin\phi\ \sin 2\psi\ \frac{\partial \sigma}{\partial r} - 2\sigma \sin\phi\ \cos 2\psi\ \frac{\partial \psi}{\partial r} - \tau \sin\theta = 0 \qquad \text{(A8)}$$

$$2\frac{\partial u}{\partial r} \tan 2\psi = \frac{\partial v}{\partial r} - \frac{v}{r} + \frac{1}{r}\ \frac{\partial u}{\partial \theta}\ . \qquad \text{(A9)}$$

The four equations (eq A1, A7, A8 and A9) are to be solved for four unknown functions, u, v, σ and ψ.

It is to be observed that the specific values of ψ at the boundary $\theta = \pm \theta_w$ result from the assumption of Coulomb friction on the boundary of the form

$$\left.\frac{N_{r\theta}}{N_{\theta\theta}}\right|_{\theta = \pm \theta_w} = \mp \tan\delta \qquad \text{(A10)}$$

where δ is the angle of friction between the ice cover and the boundary. From the eq A6 this leads to the relation

$$\psi_w = \frac{1}{2}\left[\delta + \sin^{-1}\left\{\left(\frac{\sin\delta}{\sin\phi}\right)\left(\frac{p}{p + c\cot\phi}\right)\right\}\right]. \qquad \text{(A11)}$$

Assuming the factor, $p/(p + c \cot \phi)$, is approximately equal to 1, we may evaluate ψ_w for given values of δ and ϕ. Further assuming that the velocity and stress fields are symmetrical with respect to the centerline $\theta = 0$, we see that ψ increases from zero at $\theta = 0$ to the known value of ψ_w at $\theta = \theta_w$.

Brennen and Pearce (1978) have derived a solution of eq A1, A7, A8 and A9 by expanding u, v, σ and ψ in the form of a series with increasing powers of θ. We shall follow the same procedure together with the incorporation of the simplifying assumption of radial flow, i.e. $v = 0$, and linear variation of ψ with respect to θ. Thus the functions u, σ and ψ are expanded in the form

$$u = u_0(r) + u_2(r)\left(\frac{\theta}{\theta_w}\right)^2 + 0\left(\frac{\theta^4}{\theta_w^4}\right) \qquad \text{(A12)}$$

$$\sigma = \sigma_0(r) + \sigma_2(r)\left(\frac{\theta}{\theta_w}\right)^2 + 0\left(\frac{\theta^4}{\theta_w^4}\right) \qquad \text{(A13)}$$

$$\psi = \psi_w\left(\frac{\theta}{\theta_w}\right). \qquad \text{(A14)}$$

The procedure is to expand the governing equations (eq A1, A7, A8 and A9) in powers of θ and to obtain ordinary differential equations for u_0, u_2, σ_0 and σ_2 by equating coefficients of powers of θ. The resulting equations are given below:

$$\frac{du_0}{dr} + \frac{u_0}{r} = 0 \qquad \text{(A15)}$$

$$u_2 = 2\,\psi_w\,\theta_w\,r\,\frac{du_0}{dr} \tag{A16}$$

$$(1 - \sin\phi)\,\frac{d\sigma_0}{\partial r} - \frac{2\sigma_0}{r}\,\sin\phi\left(1 + \frac{\psi_w}{\theta_w}\right) + \tau = 0 \tag{A17}$$

$$(1 + \sin\phi)\,\frac{2\sigma_2}{\theta_w} = 4\,\sigma_0\,\psi_w\,\sin\phi\left(1 + \frac{\psi_w}{\theta_w}\right) + 2r\psi_w\,\sin\phi\,\frac{d\sigma_0}{dr} + \tau r\theta_w\,. \tag{A18}$$

The solution of eq A15 is $u_0 = A/r$, and the function u_2 is obtained from eq A16. Using eq A12, the radial velocity u can be written in the form

$$u = \frac{A}{r}\,(1 - 2\psi_w\,\theta^2/\theta_w) \tag{A19}$$

where the constant A is indeterminate. This results from neglecting the inertial terms in the equations of motion (eq A2 and A3) and the weak coupling between the stress resultants and the velocity field through eq A5.

The solution of eq A17 gives

$$\frac{\sigma_0(r)}{\tau r_1} = \frac{1}{(\omega - 1)\,(1 - \sin\phi)}\left(\frac{r}{r_1}\right) + B\left(\frac{r}{r_1}\right)^{\omega} \tag{A20}$$

where $\omega = \dfrac{2\sin\phi\,(1 + \psi_w/\theta_w)}{(1 - \sin\phi)}$ and

B is a constant to be determined from the boundary conditions. The expression for $\sigma_2(r)$ may be obtained by substituting $\sigma_0(r)$ in eq A18, and thus deriving an expression for $\sigma(r, \theta)$ from eq A13 as given below:

$$\frac{\sigma}{\tau r_1} = \frac{(r/r_1)}{(\omega - 1)\,(1 - \sin\phi)}\left[1 + \left(\frac{\theta}{\theta_w}\right)^2\left\{\frac{\psi_w(3\theta_w + \psi_w)\,\sin\phi}{(1 + \sin\phi)} + \frac{\theta_w^2\,(\omega - 1)\,(1 - \sin\phi)}{2(1 + \sin\phi)}\right\}\right]$$

$$+ B\left(\frac{r}{r_1}\right)^{\omega}\left[1 + \left(\frac{\partial}{\theta_w}\right)^2\left\{\frac{\psi_w(\omega\theta_w + 2\theta_w + 2\psi_w)}{(1 + \sin\phi)}\right\}\right]\,. \tag{A21}$$

A different expression for σ results for the special case of $\omega = 1$.

In the following, the expressions for the stress resultants (N_{ij}) are derived for the special case of a frictionless boundary condition (i.e. $\delta = 0$ along $\theta = \pm\,\theta_w$ and the stress-free boundary condition (i.e. $N_{rr} = 0$ and $N_{r\theta} = 0$) along $r = r_1$ and r_2.

From eq A11, we get $\psi_w = 0$ for the case $\delta = 0$, and thus $\psi = 0$ everywhere in this region as assumed in eq A14. When $\psi = 0$, eq A6 reduces to the following:

$$N_{rr} - c\,\cot\phi = -(p + c\,\cot\phi)\,(1 - \sin\phi)$$

$$N_{\theta\theta} - c\,\cot\phi = -(p + c\,\cot\phi)\,(1 + \sin\phi)$$

$$N_{r\theta} = 0\,. \tag{A22}$$

The expression for $\sigma = (p + c\,\cot\phi)$ is derived from eq A21 as given below:

$$\frac{\sigma}{\tau r_1} = B\left(\frac{r}{r_1}\right)^{m} - \frac{r/r_1}{1\text{-}3\,\sin\phi}\left[1 - \frac{\theta^2}{2}\,\frac{1 - m}{1 + m}\right] \tag{A23}$$

where $m = \dfrac{2 \sin \phi}{1 - \sin \phi}$.

By the use of the boundary conditions $N_{rr}(r_1) = N_{rr}(r_2) = 0$, the constant B and the shear stress τ can be evaluated in terms of the geometrical and material parameters. The shear stress τ necessary to cause a critical state in the ice cover region is given below:

$$\frac{\tau (r_2 - r_1)}{c \cot \phi} = (1 - m) \Big/ \left[\left\{ \frac{r_1^m}{r_2^m - r_1^m} - \frac{r_1}{r_2 - r_1} \right\} \left\{ 1 - \frac{\theta^2}{2} \frac{1 - m}{1 + m} \right\} \right]. \tag{A24}$$

The stress resultants $(N_{rr}, N_{\theta\theta})$ are normalized with respect to $\tau (r_2 - r_1)$ which would be the maximum pressure in the ice cover region if its behavior were similar to that of a fluid (i.e. $\phi = 0$, $c = 0$) and the ice cover were blocked at $r = r_1$ (i.e. $u = 0$ at $r = r_1$). The normalized expressions for the stress resultant are given below:

$$\frac{N_{rr}}{\tau (r_2 - r_1)} = \left(\frac{1}{1 - m} \right) \left[1 - \frac{1 - m}{1 + m} \frac{\theta^2}{2} \right] \left[\frac{r - r_1}{r_2 - r_1} - \frac{r^m - r_1^m}{r_2^m - r_1^m} \right] \tag{A25}$$

$$\frac{N_{\theta\theta}}{\tau (r_2 - r_1)} = \left(\frac{1}{1 - m} \right) \left[1 - \frac{1 - m}{1 + m} \frac{\theta^2}{2} \right] \left[\frac{(m + 1) r - r_1}{r_2 - r_1} \quad \frac{(m + 1) r^m - r_1^m}{r_2^m - r_1^m} \right] . \tag{A26}$$

The graphs of $N_{rr}/\tau(r_2 - r_1)$ and $N_{\theta\theta}/\tau(r_2 - r_1)$ are given in Figure A1a with respect to r/r_1 for various values of θ/θ_w and for given values of the angle of internal friction ϕ and r_2/r_1 ratio. The distribution of stress resultants along the boundary $\theta = \pm \theta_w$ has been plotted in Figure A1b for various values of the angle of internal friction ϕ and for a given value of the r_2/r_1 ratio.

A simplified analysis, similar to that by Reimer et al. (1979), is given below. In this analysis the following assumptions have been made: 1) the unknown variables are independent of θ, 2) the flow is radial (i.e. $v = 0$), 3) the stress resultants N_{rr} and $N_{\theta\theta}$ are the principal stresses (i.e. $N_{r\theta} = 0$), and 4) the shear stress τ acts radially inward. Equations A1-A5 then reduce to the following set of equations:

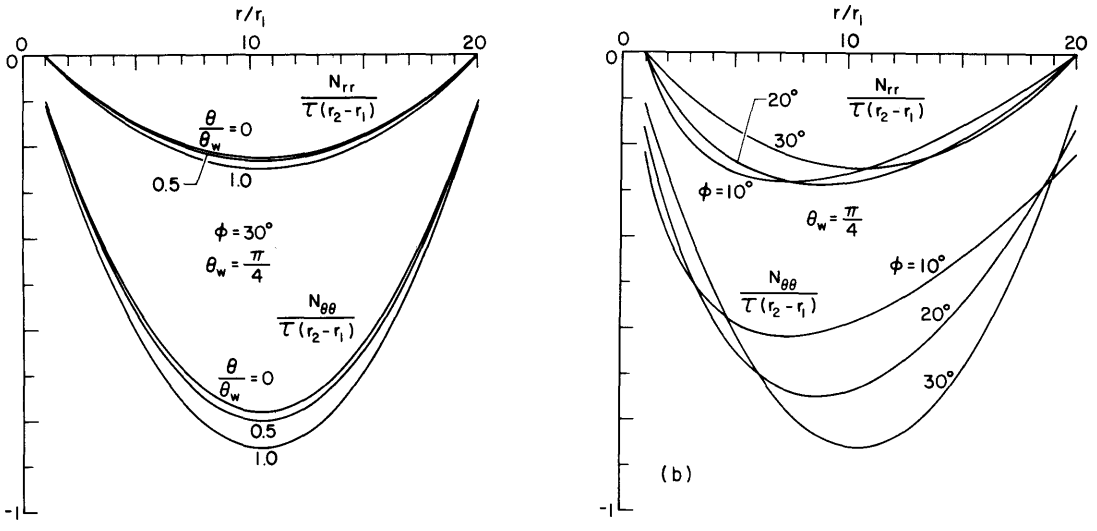

a. $\phi = 30°$, $r_2/r_1 = 20$, and $\theta/\theta_w = 0, 0.5, 1$. *b. $r_2/r_1 = 20$ and $\phi = 10°, 20°, 30°$.*

Figure A1. Distribution of stress resultants.

Continuity:

$$\frac{\partial u}{\partial r} + \frac{u}{r} = 0 \tag{A27}$$

Equilibrium:

$$\frac{\partial N_{rr}}{\partial r} + \frac{N_{rr} - N_{\theta\theta}}{r} = \tau . \tag{A28}$$

Yield criterion:

$$\frac{N_{rr} - c \cot \phi}{N_{\theta\theta} - c \cot \phi} = \frac{1 - \sin \phi}{1 + \sin \phi} . \tag{A29}$$

The solution of eq A27 is $u = A/r$ where the constant of integration A is indeterminate. Eliminating $N_{\theta\theta}$ from eq A28 with the help of eq A29 we get

$$\frac{\partial}{\partial r} (N_{rr} - c \cot \phi) - m (N_{rr} - c \cot \phi)/r = \tau \tag{A30}$$

where $m = 2 \sin \phi/(1 - \sin \phi)$. The solution of eq A30 may be written in the following form:

$$\frac{N_{rr} - c \cot \phi}{\tau r_1} = B \left(\frac{r}{r_1}\right)^m + \frac{r/r_1}{(1 - m)} . \tag{A31}$$

By the use of the boundary conditions $N_{rr}(r_1) = N_{rr}(r_2) = 0$, we may evaluate B and the shear stress τ in terms of the material and geometrical parameters of the ice cover region. The shear stress necessary to cause a critical state in the ice region is given by

$$\frac{\tau(r_2 - r_1)}{c \cot \phi} = (1 - m)/ \left[\frac{r_1^m}{r_2^m - r_1^m} - \frac{r_1}{r_2 - r_1}\right]. \tag{A32}$$

The above expression is identical to those given by Sodhi (1975) and Reimer et al. (1979). The expressions for N_{rr} and $N_{\theta\theta}$ are normalized with respect to $\tau(r_2 - r_1)$ and are given below:

$$\frac{N_{rr}}{\tau(r_2 - r_1)} = \frac{1}{(1 - m)} \left[\frac{r - r_1}{r_2 - r_1} - \frac{r^m - r_1^m}{r_2^m - r_1^m}\right] \tag{A33}$$

$$\frac{N_{\theta\theta}}{\tau(r_2 - r_1)} = \frac{1}{(1 - m)} \left[\frac{(1 + m) r - r_1}{r_2 - r_1} - \frac{(1 + m) r^m - r_1^m}{r_2^m - r_1^m}\right] . \tag{A34}$$

The above expressions are identical to eq A25 and A26 except for a factor involving an expression of θ.

APPENDIX B. MONTHLY SUMMARY OF WIND DATA AT PORT HURON.

Wind direction	Percentage of time from a given direction	Wind speed and duration in percentage (mph) 0-10	10-20	20-30	30-40	40-50	>50
January 1976							
N	0.8	0	0	100	0	0	0
NNE	1.6	50	50	0	0	0	0
NE	0.8	100	0	100	0	0	0
ENE	4.0	80	20	0	0	0	0
E	0.8	100	0	0	0	0	0
ESE	3.2	25	75	0	0	0	0
SE	0.8	0	100	0	0	0	0
SSE	11.3	43	57	0	0	0	0
S	3.2	75	25	0	0	0	0
SSW	25.8	19	81	0	0	0	0
SW	2.4	67	33	0	0	0	0
WSW	8.9	64	36	0	0	0	0
W	2.4	67	33	0	0	0	0
WNW	26.6	52	48	0	0	0	0
NW	4.0	60	40	0	0	0	0
NNW	3.2	25	75	0	0	0	0
February 1976							
N	0.9	100	0	0	0	0	0
NNE	4.3	40	60	0	0	0	0
NE	0.0	0	0	0	0	0	0
ENE	3.4	75	25	0	0	0	0
E	0.9	0	100	0	0	0	0
ESE	4.3	40	40	20	0	0	0
SE	2.2	17	83	0	0	0	0
S	0.0	0	0	0	0	0	0
SSW	26.7	19	81	0	0	0	0
SW	1.7	100	0	0	0	0	0
WSW	9.5	45	55	0	0	0	0
W	3.4	45	55	0	0	0	0
WNW	24.1	71	25	4	0	0	0
NW	6.0	86	14	0	0	0	0
NNW	6.9	13	75	13	0	0	0
March 1976							
N	3.0	100	0	0	0	0	0
NNE	10.0	40	60	0	0	0	0
NE	102	100	0	0	0	0	0
ENE	9.0	100	0	0	0	0	0
E	0.0	0	0	0	0	0	0
ESE	4.0	75	25	0	0	0	0
SE	1.0	0	100	0	0	0	0
SSE	3.0	67	33	0	0	0	0
S	1.0	0	100	0	0	0	0
SSW	28.0	36	61	0	0	0	0
SW	2.0	100	0	0	0	0	0
WSW	9.0	33	56	11	0	0	0
W	3.0	33	67	0	0	0	0
WNW	21.0	81	19	0	0	0	0
NW	0.0	0	0	0	0	0	0
NNW	5.0	0	100	0	0	0	0
December 1976							
N	0.0	0	0	0	0	0	0
NNE	0.0	0	0	0	0	0	0
NE	0.8	100	0	0	0	0	0
ENE	0.8	100	0	0	0	0	0
E	0.0	0	0	0	0	0	0
ESE	1.6	100	0	0	0	0	0
SE	2.4	100	0	0	0	0	0
SSE	8.1	50	50	0	0	0	0
S	0.8	100	0	0	0	0	0
SSW	25.8	41	50	0	0	0	0
SW	25.8	88	50	0	0	0	0
WSW	16.9	76	24	0	0	0	0
W	16.9	86	24	0	0	0	0
WNW	21.8	52	48	0	0	0	0
NW	4.0	60	40	0	0	0	0
NNW	4.8	67	33	0	0	0	0
January 1977							
N	0.8	0	100	0	0	0	0
NNE	0.8	0	0	100	0	0	0
NE	0.8	0	100	0	0	0	0
ENE	0.8	100	0	0	0	0	0
E	0.0	0	0	0	0	0	0
ESE	0.0	0	0	0	0	0	0
SE	0.0	0	0	0	0	0	0
SSE	1.6	0	100	0	0	0	0
S	1.6	50	50	0	0	0	0

Wind direction	Percentage of time from a given direction	Wind speed and duration in percentage (mph) 0-10	10-20	20-30	30-40	40-50	>50
January 1977 (cont.)							
SSW	24.2	57	43	0	0	0	0
SW	8.1	50	50	0	0	0	0
WSW	29.0	53	44	3	0	0	0
W	6.5	88	13	0	0	0	0
WNW	19.4	42	58	0	0	0	0
NW	5.6	71	29	0	0	0	0
NNW	0.8	100	0	0	0	0	0
February 1977							
N	0.0	0	0	0	0	0	0
NNE	6.3	86	14	0	0	0	0
NE	1.8	50	50	0	0	0	0
ENE	0.9	0	100	0	0	0	0
E	0.0	0	0	0	0	0	0
ESE	2.7	0	100	0	0	0	0
SE	0.9	0	100	0	0	0	0
SSE	2.7	100	0	0	0	0	0
S	3.6	50	50	0	0	0	0
SSW	19.6	36	59	5	0	0	0
SW	6.3	57	43	0	0	0	0
WSW	16.1	67	33	0	0	0	0
W	5.4	100	0	0	0	0	0
WNW	23.2	69	31	0	0	0	0
NW	6.3	100	0	0	0	0	0
NNW	4.5	20	60	20	0	0	0
March 1977							
N	1.6	100	0	0	0	0	0
NNE	8.1	60	10	20	10	0	0
NE	1.6	50	0	50	0	0	0
ENE	2.4	0	67	33	0	0	0
E	0.0	0	0	0	0	0	0
ESE	4.8	33	67	0	0	0	0
SE	2.4	33	67	0	0	0	0
SSE	20.2	32	60	0	0	0	0
S	0.9	0	100	0	0	0	0
SSW	23.4	55	41	0	0	0	0
SW	1.6	50	50	0	0	0	0
WSW	12.9	88	6	6	0	0	0

Wind direction	Percentage of time from a given direction	Wind speed and duration in percentage (mph) 0-10	10-20	20-30	30-40	40-50	>50
March 1977 (cont.)							
W	3.2	60	40	0	0	0	0
WNW	8.1	60	40	0	0	0	0
NW	5.6	14	0	0	0	0	0
NNW	5.6	14	57	14	14	0	0
November 1977							
N	3.6	25	25	50	0	0	0
NNW	6.3	71	29	0	0	0	0
NE	2.7	67	33	0	0	0	0
ENE	3.6	100	0	0	0	0	0
E	3.6	75	25	0	0	0	0
ESE	8.0	89	11	0	0	0	0
SE	8.9	70	30	0	0	0	0
SSE	2.7	67	33	0	0	0	0
S	10.7	58	42	0	0	0	0
SSW	8.0	44	56	0	0	0	0
SW	12.5	64	36	0	0	0	0
WSW	8.0	67	33	0	0	0	0
W	9.8	55	45	0	0	0	0
WNW	6.3	57	43	0	0	0	0
NW	5.4	33	50	17	0	0	0
NNW	0.0	0	0	0	0	0	0
December 1977							
N	1.6	50	0	50	0	0	0
NNE	1.6	50	0	0	50	0	0
NE	1.6	50	0	0	50	0	0
ENE	1.6	50	0	50	0	0	0
E	2.4	100	0	0	0	0	0
ESE	8.1	20	80	0	0	0	0
SE	3.2	50	50	0	0	0	0
SSE	4.0	40	60	0	0	0	0
S	13.7	29	71	0	0	0	0
SSW	13.7	65	35	0	0	0	0
SW	13.7	76	18	0	0	0	0
WSW	12.9	76	19	6	0	0	0
W	7.3	44	56	0	0	0	0
WNW	8.9	64	36	0	0	0	0
NW	3.2	75	25	0	0	0	0
NNW	2.4	100	0	0	0	0	0

Wind direction	Percentage of time from a given direction	Wind speed and duration in percentage (mph) 0-10	10-20	20-30	30-40	40-50	>50
January 1978							
N	4.8	50	17	33	0	0	0
NNE	12.9	13	63	25	0	0	0
NE	3.2	25	50	25	0	0	0
ENE	2.4	100	0	0	0	0	0
E	2.4	67	33	0	0	0	0
ESE	4.0	100	0	0	0	0	0
SE	2.4	100	0	0	0	0	0
SSE	0.0	0	0	0	0	0	0
S	4.0	60	40	0	0	0	0
SSW	11.3	79	21	0	0	0	0
SW	10.5	100	0	0	0	0	0
WSW	7.3	67	33	0	0	0	0
W	13.7	65	35	0	0	0	0
WNW	14.5	44	50	6	0	0	0
NW	4.0	60	40	0	0	0	0
NNW	2.4	67	33	0	0	0	0
February 1978							
N	13.4	33	47	20	0	0	0
NNE	4.5	60	20	20	0	0	0
NE	3.6	75	25	0	0	0	0
ENE	1.8	100	0	0	0	0	0
E	0.0	0	0	0	0	0	0
ESE	0.9	100	0	0	0	0	0
SE	0.0	0	0	0	0	0	0
SSE	2.7	100	0	0	0	0	0
S	5.4	100	0	0	0	0	0
SSW	11.6	100	0	0	0	0	0
SW	15.2	100	00	0	0	0	0
WSW	6.3	100	0	0	0	0	0
W	15.2	94	6	0	0	0	0
WNW	10.7	92	8	0	0	0	0
NW	4.5	100	0	0	0	0	0
NNW	4.5	80	20	0	0	0	0
March 1978							
N	10.5	92	0	8	0	0	0
NNE	7.3	67	33	0	0	0	0
NE	1.6	100	0	0	0	0	0

Wind direction	Percentage of time from a given direction	Wind speed and duration in percentage (mph) 0-10	10-20	20-30	30-40	40-50	>50
March 1978 (cont.)							
ENE	4.0	40	60	0	0	0	0
E	4.8	100	0	0	0	0	0
ESE	0.0	0	0	0	0	0	0
SE	4.0	40	60	0	0	0	0
SSE	4.8	83	17	0	0	0	0
S	4.8	83	17	0	0	0	0
SSW	10.5	85	15	0	0	0	0
SW	7.3	100	0	0	0	0	0
WSW	4.0	80	20	0	0	0	0
W	12.9	88	13	0	0	0	0
WNW	12.9	94	6	0	0	0	0
NW	4.8	100	0	0	0	0	0
NNW	5.6	100	0	0	0	0	0
N	0.0	0	0	0	0	0	0
NNE	4.2	80	20	0	0	0	0
NE	1,7	50	50	0	0	0	0
ENE	2.5	67	33	0	0	0	0
E	1.7	0	100	0	0	0	0
ESE	16.7	45	55	0	0	0	0
SE	3.3	100	0	0	0	0	0
SSE	3.3	50	0	50	0	0	0
S	2.5	67	33	0	0	0	0
SSW	20.0	63	38	0	0	0	0
SW	6.7	63	38	0	0	0	0
WSW	14.2	53	41	6	0	0	0
W	5.8	71	29	0	0	0	0
WNW	12.5	60	40	0	0	0	0
NW	2.5	100	0	0	0	0	0
NNW	2.5	100	0	0	0	0	0
December 1978							
N	0.8	100	0	0	0	0	0
NNE	2.4	67	33	0	0	0	0
NE	0.0	0	0	0	0	0	0
ENE	0.0	0	0	0	0	0	0
E	0.8	100	0	0	0	0	0
ESE	12.1	47	53	0	0	0	0
SE	0.8	100	0	0	0	0	0
SSE	6.5	38	63	0	0	0	0
S	1.6	50	50	0	0	0	0

Wind direction	Percentage of time from a given direction	Wind speed and duration in percentage (mph) 0-10	10-20	20-30	30-40	40-50	>50
December 1978 (cont.)							
SSW	16.9	24	76	0	0	0	0
SW	8.1	60	40	0	0	0	0
WSW	23.4	76	21	3	0	0	0
W	1.6	0	100	0	0	0	0
WNW	21.0	65	35	0	0	0	0
NW	3.2	50	50	0	0	0	0
NNW	0.8	100	0	0	0	0	0
January 1979							
N	3.2	75	25	0	0	0	0
NNE	2.4	67	0	33	0	0	0
NE	1.6	50	50	0	0	0	0
ENE	2.4	100	0	0	0	0	0
E	2.4	67	33	0	0	0	0
ESE	8.1	50	50	0	0	0	0
SE	2.4	100	0	0	0	0	0
SSE	4.8	83	17	0	0	0	0
S	0.8	100	0	0	0	0	0
SSW	7.3	56	44	0	0	0	0
SW	4.0	40	60	0	0	0	0
WSW	16.1	50	50	0	0	0	0
W	3.2	100	0	0	0	0	0
WNW	22.6	54	43	4	0	0	0
NW	1.6	50	50	0	0	0	0
NNW	16.9	33	67	0	0	0	0
February 1979							
N	0.9	100	0	0	0	0	0
NNE	0.0	0	0	0	0	0	0
NE	0.0	0	0	0	0	0	0
ENE	0.0	0	0	0	0	0	0
E	0.0	0	0	0	0	0	0
ESE	60.7	99	1	0	0	0	0
SE	2.7	100	0	0	0	0	0
SSE	3.6	100	0	0	0	0	0
S	0.9	100	0	0	0	0	0
SSW	5.4	67	33	0	0	0	0
SW	1.8	50	50	0	0	0	0
WSW	7.1	50	50	0	0	0	0

Wind direction	Percentage of time from a given direction	Wind speed and duration in percentage (mph) 0-10	10-20	20-30	30-40	40-50	>50
February 1979 (cont.)							
W	3.6	50	50	0	0	0	0
WNW	8.9	50	50	0	0	0	0
NW	1.8	100	0	0	0	0	0
NNW	2.7	67	33	0	0	0	0
March 1979							
N	2.4	100	0	0	0	0	0
NNE	15.3	84	16	0	0	0	0
NE	1.6	100	0	0	0	0	0
ENE	3.2	100	0	0	0	0	0
E	0.8	100	0	0	0	0	0
ESE	4.8	67	33	0	0	0	0
SE	4.0	100	0	0	0	0	0
SSE	16.9	33	62	0	0	0	0
S	0.8	100	0	0	0	0	0
SSW	15.3	26	74	0	0	0	0
SW	5.6	71	29	0	0	0	0
WSW	2.4	67	33	0	0	0	0
WNW	10.5	62	38	0	0	0	0
NW	2.4	67	33	0	0	0	0
NNW	4.8	83	17	0	0	0	0
November 1979							
N	4.2	0	80	20	0	0	0
NNE	0.0	0	0	0	0	0	0
NE	0.8	0	100	0	0	0	0
ENE	0.8	0	100	0	0	0	0
E	0.8	0	100	0	0	0	0
ESE	4.2	40	60	0	0	0	0
SE	1.7	100	0	0	0	0	0
SSE	5.8	100	0	0	0	0	0
S	4.2	100	0	0	0	0	0
SSW	24.2	55	38	7	0	0	0
SW	10.8	77	23	0	0	0	0
WSW	19.2	65	35	0	0	0	0
W	5.0	100	0	0	0	0	0
WNW	10.0	75	25	0	0	0	0
NW	2.5	67	0	33	0	0	0
NNW	5.8	71	29	0	0	0	0

Wind direction	Percentage of time from a given direction	Wind speed and duration in percentage (mph) 0-10	10-20	20-30	30-40	40-50	>50
December 1979							
N	0.8	100	0	0	0	0	0
NNE	4.0	20	0	20	0	0	0
NE	0.8	100	0	0	0	0	0
ENE	0.0	0	0	0	0	0	0
E	0.8	100	0	0	0	0	0
ESE	7.3	89	11	0	0	0	0
SE	4.0	100	0	0	0	0	0
SSE	3.2	50	50	0	0	0	0
S	4.8	83	17	0	0	0	0
SSW	25.0	29	65	6	0	0	0
SW	5.6	86	14	0	0	0	0
WSW	12.1	80	20	0	0	0	0
W	3.2	50	50	0	0	0	0
WNW	14.5	83	17	0	0	0	0
NW	4.8	100	0	0	0	0	0
NNW	8.9	64	18	18	0	0	0
January 1980							
N	0.0	0	0	0	0	0	0
NNE	5.6	71	29	0	0	0	0
NE	1.6	50	50	0	0	0	0
ENE	2.4	0	100	0	0	0	0
E	0.0	0	0	0	0	0	0
ESE	3.2	100	0	0	0	0	0
SE	2.4	67	33	0	0	0	0
SSE	12.1	27	60	13	0	0	0
S	3.2	25	50	25	0	0	0
SSW	8.9	27	55	18	0	0	0
SW	2.4	33	67	0	0	0	0
WSW	13.7	76	18	0	0	0	0
W	6.5	75	25	0	0	0	0
WNW	28.2	66	34	0	0	0	0
NW	3.2	75	25	0	0	0	0
NNW	6.5	50	50	0	0	0	0
February 1980							
N	2.6	33	33	33	0	0	0
NNE	3.4	75	0	0	25	0	0
NE	1.7	100	0	0	0	0	0
ENE	1.7	100	0	0	0	0	0
E	2.6	67	33	0	0	0	0

Wind direction	Percentage of time from a given direction	Wind speed and duration in percentage (mph) 0-10	10-20	20-30	30-40	40-50	>50
February 1980							
ESE	10.3	75	25	0	0	0	0
SE	0.9	100	0	0	0	0	0
SSE	4.3	100	0	0	0	0	0
S	0.9	100	0	0	0	0	0
SSW	18.1	43	57	0	0	0	0
SW	4.3	80	20	0	0	0	0
WSW	10.3	67	33	0	0	0	0
W	0.9	100	0	0	0	0	0
WNW	22.4	69	31	0	0	0	0
NW	5.2	83	17	0	0	0	0
NNW	10.3	58	42	0	0	0	0
March 1980							
N	1.6	50	50	0	0	0	0
NNE	14.5	39	50	11	0	0	0
NE	4.0	60	20	20	0	0	0
ENE	4.8	17	83	0	0	0	0
E	0.8	100	0	0	0	0	0
ESE	4.0	40	60	0	0	0	0
SE	2.4	100	0	0	0	0	0
SSE	16.1	40	55	0	0	0	0
S	3.2	75	25	0	0	0	0
WSW	4.8	33	67	0	0	0	0
W	4.8	67	33	0	0	0	0
WNW	12.9	44	56	0	0	0	0
NW	4.8	33	67	0	0	0	0
NNW	10.5	62	23	15	0	0	0